Supporting Information

Experimental

1. Preparation of the Electrolytes

The D7 electrolyte was prepared as follows: First, 3 mol $ZnSO_4$ was dissolved in 1 L deionized water to obtain 3 M $ZnSO_4$ electrolyte. Subsequently, dextran with a molecular weight of 70000 was added to the electrolyte at a mass fraction of 0.5 $g\cdot L^{-1}$ to obtain the D7 electrolyte. D2, D4, D10, and D15 electrolytes were prepared using the same procedure but with dextran molecular weights adjusted to 20000, 40000, 100 000, and 150000, respectively.

2. Preparation of MnO_2

MnO_2 cathodes were fabricated via electrochemical deposition using titanium foil as the current collector and a saturated calomel electrode as the reference electrode. The deposition was performed in a mixed solution containing 0.1 mol L^{-1} $MnSO_4$ and 0.1 mol L^{-1} NaAc, with a voltage window of 0.2–0.8 V and a scan rate of 20 mV s^{-1}. The deposited electrodes were rinsed repeatedly with deionized water and dried at 80°C under vacuum for 6 hours. The MnO_2 mass loading was standardized at 0.5 mg cm^{-2}.

2. Material Characterization

Morphological analysis was conducted using field-emission scanning electron microscopy (FESEM, HITACHI SU8100). Crystal phases were characterized by X-ray diffraction (XRD, Holland Analysis PRO PW3040/60) with Cu Kα radiation at a scanning rate of 10° min^{-1}. X-ray photoelectron spectroscopy (XPS) measurements were performed on an Escalab250Xi system using monochromatic Al Kα radiation (hv = 1486.6 eV). Fourier-transform infrared spectroscopy (FTIR, Shimadzu IRTracer-100) was employed with a resolution of 4 cm^{-1}, MIRTGS detector, and infrared light source. Raman spectra were acquired using a Horiba LabRAM HR Evolution spectrometer with a 532 nm laser.

3. *Electrochemical Testing*

CR2032 coin cells were assembled as follows: Zn//Zn symmetric cells: zinc foils as both electrodes; Zn//Ti cells: zinc foil (anode) and titanium foil (cathode); Zn//MnO_2 full cells: zinc foil (anode) and MnO_2 cathode. Electrolytes (3 M $ZnSO_4$ or 3 M $ZnSO_4$ with 0.5 g L^{-1} dextran) were injected (400 μL per cell), and a glass fiber separator (Whatman) was used under 500 psi compression. Cyclic voltammetry (CV) and electrochemical impedance spectroscopy (EIS) were performed on a CHI electrochemical workstation. Tafel plots were measured in a three-electrode system with zinc foil (working electrode), platinum mesh (counter electrode), and Ag/AgCl (reference electrode). Linear sweep voltammetry (LSV) for full cells was conducted at 1 mV s^{-1}. Chronoamperometry (CA) tests were performed on symmetric cells at a constant overpotential of -150 mV. Cycling performance was evaluated using a LAND battery tester. Zinc ion transference numbers ($t_{Zn^{2+}}$) were calculated via the Evans method:

$$t_{Zn^{2+}} = \frac{I_S(\Delta V - I_0 R_0)}{I_0(\Delta V - I_S R_S)} \quad (1)$$

Where I_0/I_s and R_0/R_s represent the initial/final current density and charge transfer resistance before and after the polarization test, respectively, and ΔV is the constant polarization voltage in the CA test.

4. Computational methods of MD

MD simulations were performed by the GROMACS software. The forced field parameters originate from the gromos54a7 force fields. The size of the box is 10 × 10 ×10 nm^3, with periodic boundary conditions in all three directions. The simulation system with DEX additives contains 7180 H_2O, 755 Zn^{2+}, 755 $SO4^{2-}$ and 5 DEX, and the pure $ZnSO_4$ system includes 7180 H_2O, 755 $Zn^{2+}$and 755 $SO4^{2-}$. Particle-Mesh-Ewald (PME) methods were utilized to compute the electrostatic interactions.[1] A cutoff length of 1.0 nm was used in the calculation of electrostatic interactions and non-electrostatic (van der Waals) interactions in real space, and the integration time step was 1 fs.[2] The system was annealed from 0 to 298 K in 0.5 ns, and retained a constant temperature for another 1.0 ns to reach equilibrium. The temperature and pressure coupling were performed in V-rescale and Berendsen method, respectively. A 10-ns production simulation was then carried out for trajectory analysis, during which the pressure coupling method was switched to the Parrinello–Rahman barostat to allow for more accurate pressure fluctuations under NPT conditions.

After the production simulation, structural properties of the system were investigated through the calculation of the radial distribution function (RDF), g(r), and coordination number, n(r), to evaluate the molecular-level spatial organization and solvation structure, particularly around Zn^{2+}.[3] RDFs were computed using atomic trajectories extracted from the production phase, sampled at 1 fs intervals to ensure sufficient temporal resolution. These functions describe the probability of finding an atom at a distance r from a reference particle, normalized by the bulk density. The coordination number, representing the cumulative number of atoms surrounding a central ion within a given radius, was determined by integrating the RDF according to the following expressions:

$$g(r) = \frac{dn(r)}{4\pi dr\rho r} \quad n(r) = \int_0^r 4\pi r^2 g(r)\, \rho(r)\, dr \tag{2}$$

where ρ(*r*) is the local density of atoms.

5. DFT calculations

The density functional theory (DFT) calculations were performed using the DMol3 module. The electronic exchange-correlation interactions were described by the Perdew-Burke-Ernzerhof (PBE) functional within the generalized gradient approximation (GGA).[4-6] The nuclear processing method uses all-electron relativistic effects.[7] The double numerical plus polarization (DNP) basis set was employed, with an orbital cutoff radius set to 3.5 Å.[8] A Fine level of numerical integration accuracy was applied, and the self-consistent field (SCF) convergence criterion was set to 1.0×10^{-6} eV/atom.[9] During geometry optimization, the energy convergence threshold was set to 1.0×10^{-5} Ha, the force convergence threshold was set to 0.002 Ha/Å, and the maximum atomic displacement threshold was set to 0.005 Å. Based on the optimized molecular structure, a single-point energy calculation was performed, and the

Molecular Orbital functionality was enabled to extract information on the highest occupied molecular orbital (HOMO) and lowest unoccupied molecular orbital (LUMO).[10] For orbital occupation calculations, a 0.005 Ha smear was applied to accelerate SCF convergence, and the spatial distribution of frontier molecular orbitals was visualized using the Visualize module. The binding energy between Zn^{2+} and different molecules was defined as the following equation:

$$E_{bind} = E_{complex} - \left(E_{Zn^{2+}} + E_{molecule}\right) \tag{3}$$

Where E_{bind} is the energy released (or absorbed) upon the formation of the complex between Zn^{2+} and the molecule. $E_{complex}$ is the total energy of the Zn^{2+}-molecule complex., $E_{Zn^{2+}}$ is the energy of the isolated Zn^{2+}, while $E_{Molecule}$ is the energy of the free ligand molecule.

References

[1] M. Yasir, J. Park, Y. Lee, E.-T. Han, W. S. Park, J.-H. Han, Y.-S. Kwon, H.-J. Lee and W. Chun, Int. J. Mol. Sci., 2023, 24, 16990.

[2] R. Wang, M. Yao, M. Yang, J. Zhu, J. Chen and Z. Niu, Proc. Natl. Acad. Sci. U.S.A., 2023, 120, e2221980120.

[3] G. Liang, B. Liang, A. Chen, J. Zhu, Q. Li, Z. Huang, X. Li, Y. Wang, X. Wang, B. Xiong, X. Jin, S. Bai, J. Fan and C. Zhi, Nat. Commun., 2023, 14, 1-11.

[4] P. E. Blöchl, Phys. Rev. B, 1994, 50, 17953-17979.

[5] G. Kresse and J. Furthmüller, Phys. Rev. B, 1996, 54, 11169-11186.

[6] J. P. Perdew, K. Burke and M. Ernzerhof, Phys. Rev. Lett., 1996, 77, 3865-3868.

[7] D. D. Koelling and B. N. Harmon, J. Phys. C: Solid State Phys., 1977, 10, 3107.

[8] Z.-B. Zhou, P.-J. Tian, J. Yao, Y. Lu, Q.-Y. Qi and X. Zhao, Nat. Commun., 2022, 13, 1-8.

[9] M. G. Mohamed, M. H. Elsayed, Y. Ye, M. M. Samy, A. E. Hassan, T. H. Mansoure, Z. Wen, H.-H. Chou, K.-H. Chen and S.-W. Kuo, Polymers, 2022, 15, 182-198.

[10] X.-Q. Liao, C.-M. Zhang, F. Li, Z.-L. Yin, G.-C. Liu and J.-G. Yu, New J. Chem. , 2021, 45, 3160-3168.

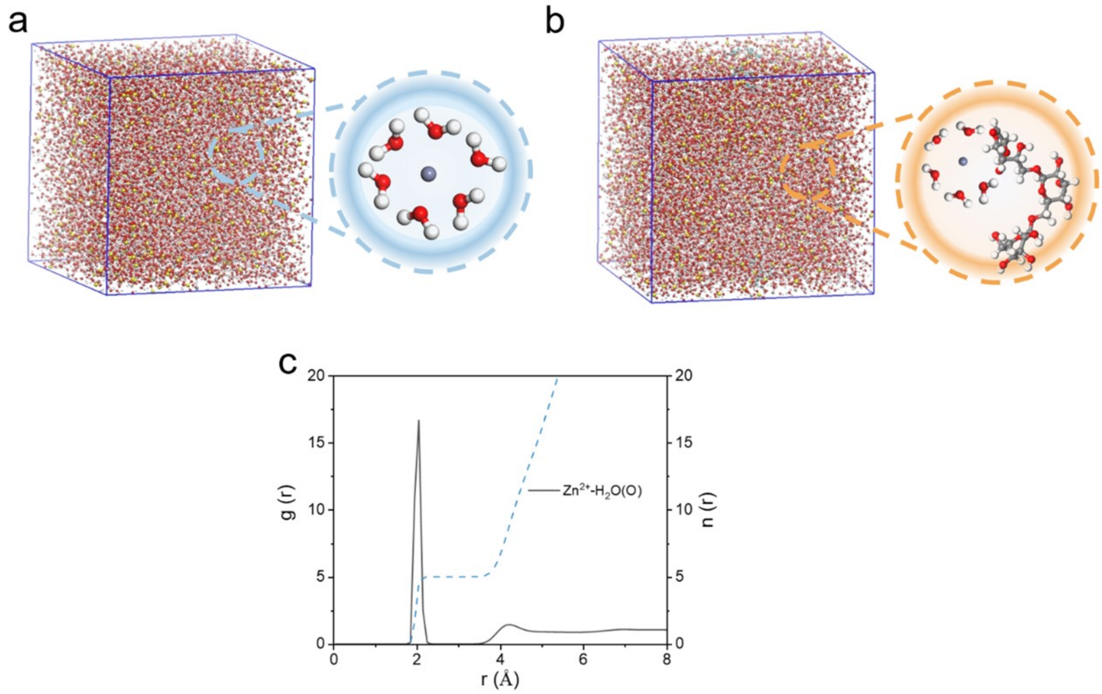

Fig. S1. The boxes of molecular dynamics simulations with main solvated structure of Zn^{2+} in a) $ZnSO_4$ and b) DEX /$ZnSO_4$. c) The RDF for Zn^{2+}- DEX(O) and Zn^{2+}- H_2O (O) in $ZnSO_4$.

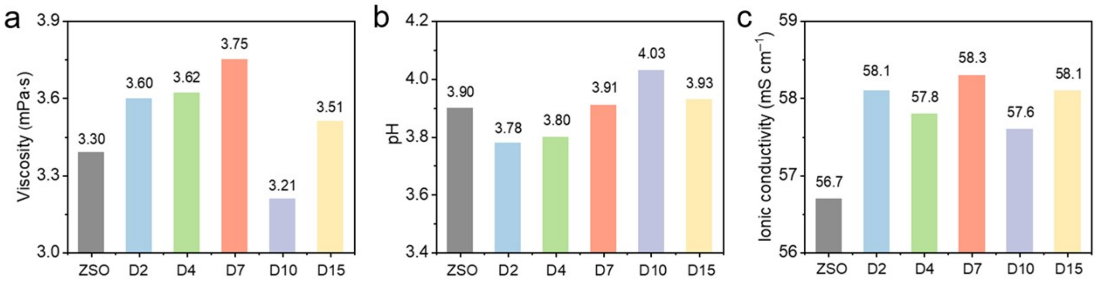

Fig. S2. D2, D4, D7, D10, D15 and ZSO (a) viscosity, (b) pH and (c) ionic conductivity.

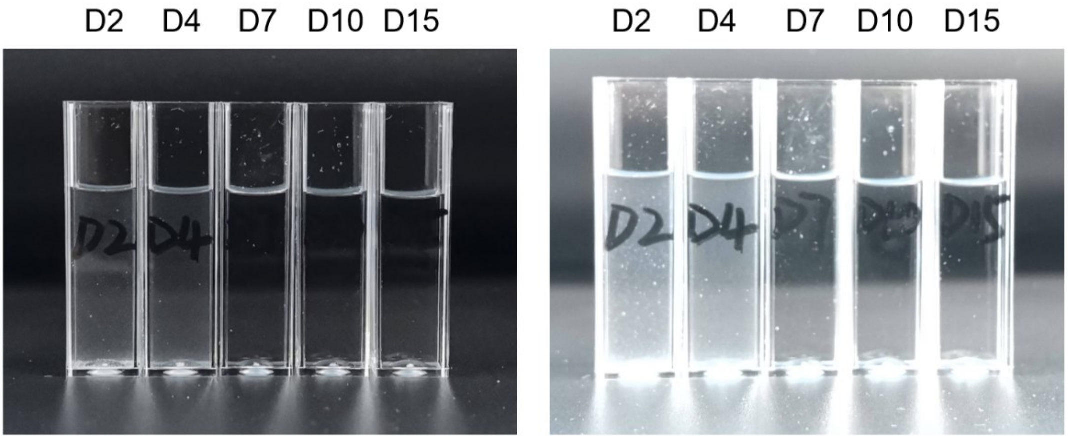

Fig. S3. Appearance comparison photos of D2, D4, D7, D10 and D15 electrolytes in a colorimetric dish under different lighting conditions.

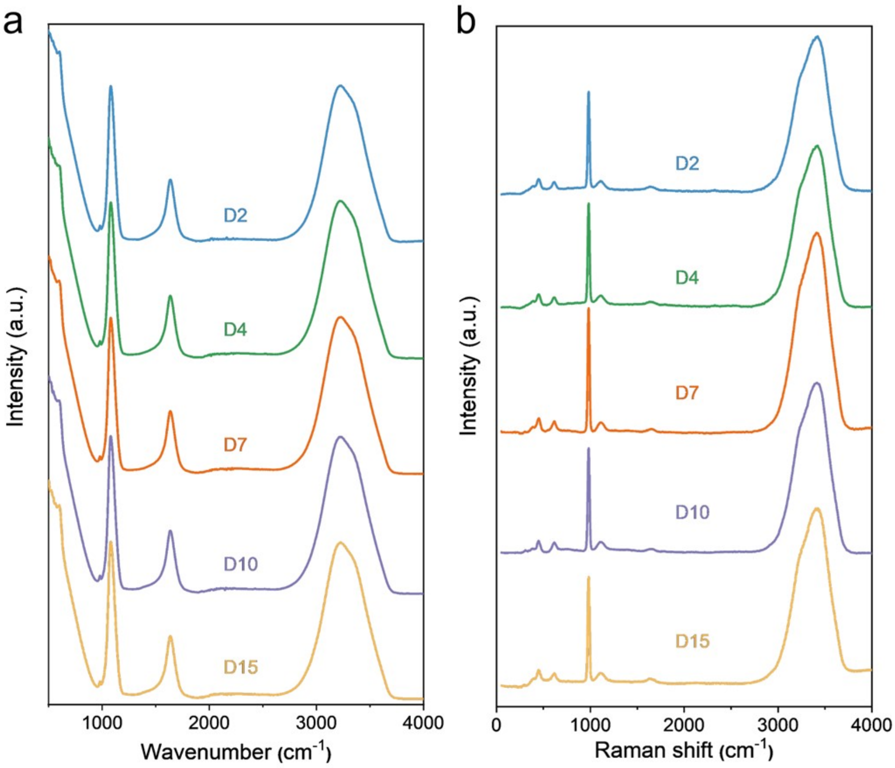

Fig. S4. (a) FTIR and (b) Raman spectra of D2, D4, D7, D10 and D15.

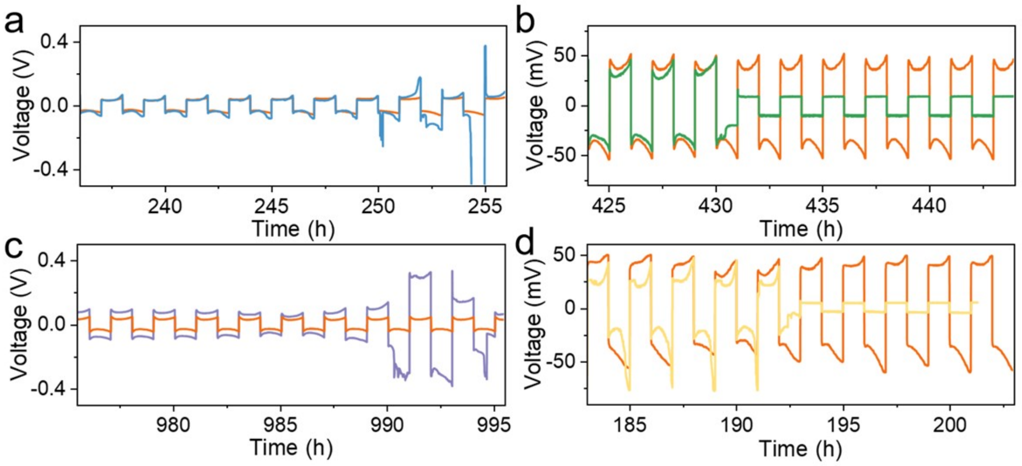

Fig. S5. (a) D2, (b)D4, (c)D10, (d) D15 failure voltage curve details.

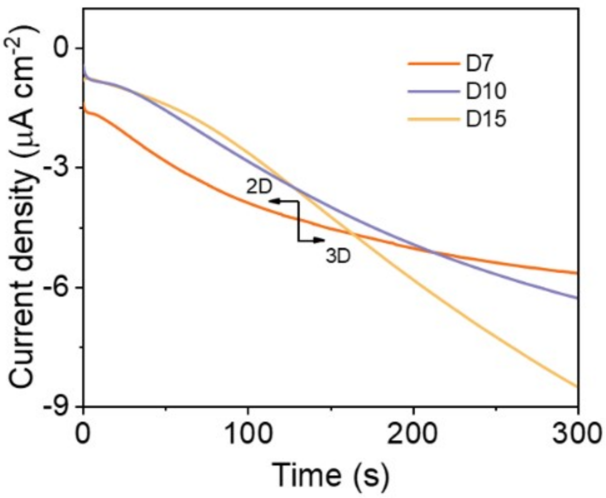

Fig. S6. Enlarged View of the CA Curve Details for D7, D10, and D15.

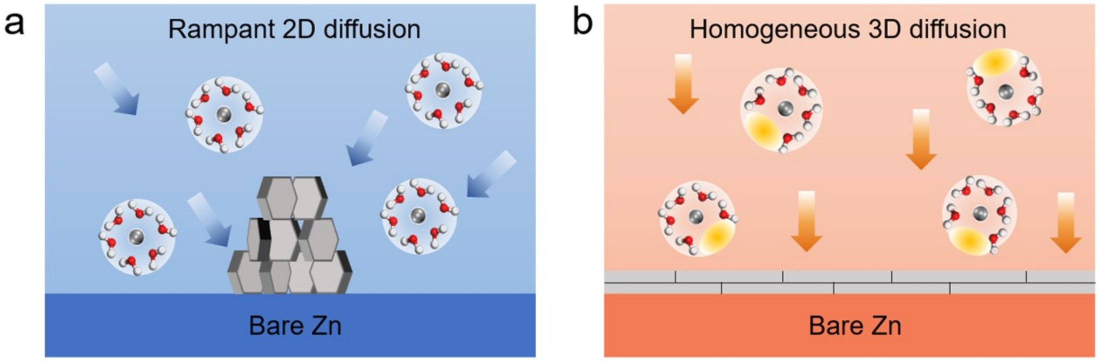

Fig. S7. Schematic Illustration of 2D and 3D Diffusion Mechanisms.

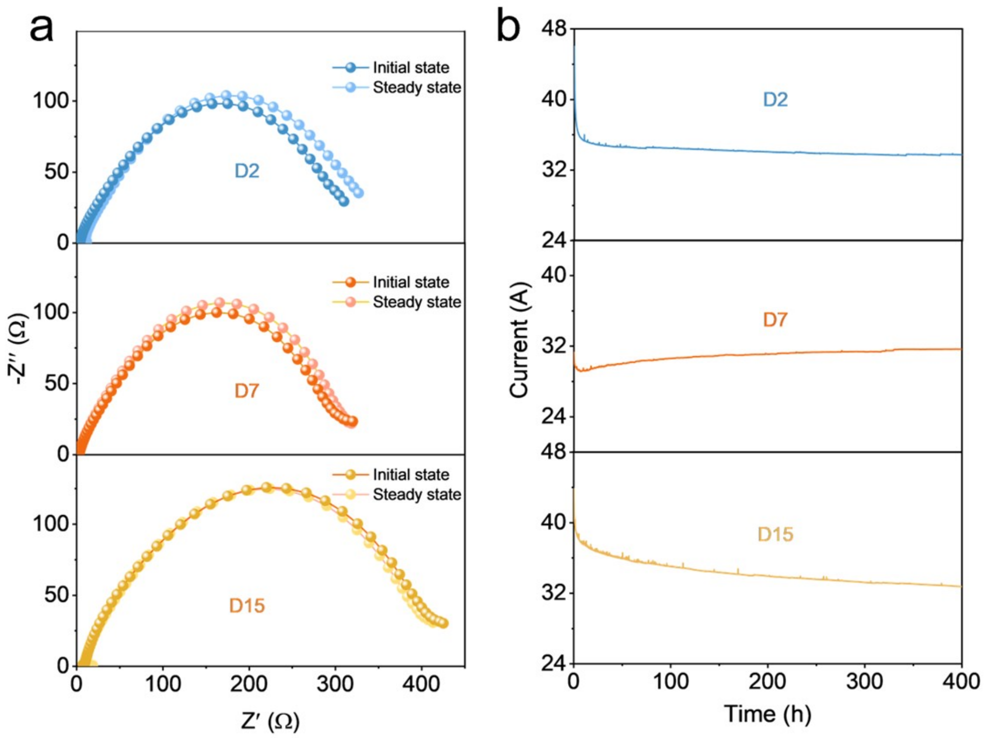

Fig. S8. (a) EIS curves of Zn//Zn-symmetric batteries before and after polarization in electrolyte D2, D7 and D15; (b) CA curve corresponding to 10 mV voltage applied at room temperature.

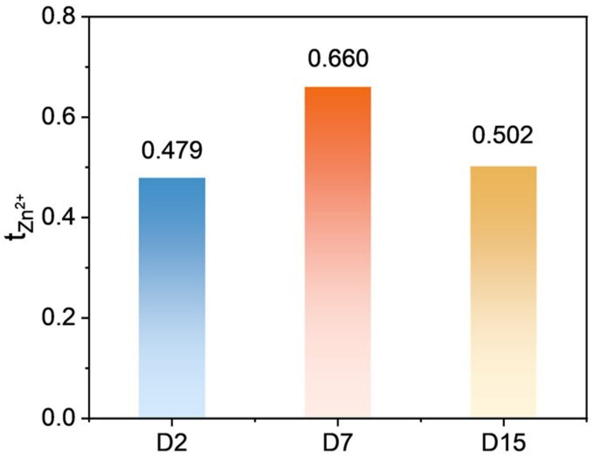

Fig. S9. Zn^{2+} diffusion coefficient ($t_{Zn^{2+}}$) of Zn//Zn-symmetric batteries in electrolyte D2, D7 and D15.

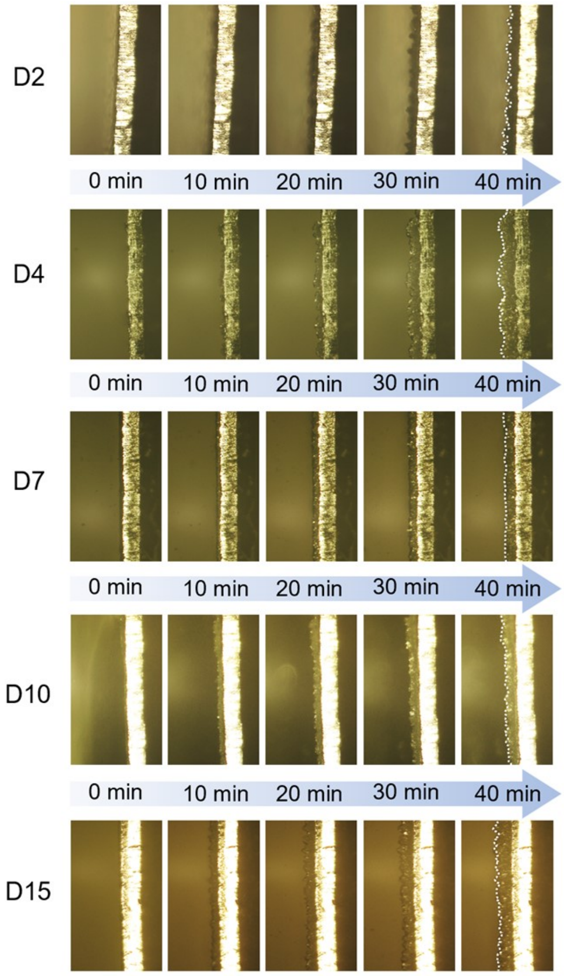

Fig. S10. The surface morphology of zinc anode deposited in D2, D4, D7, D10 and D15 electrolytes at 1 mA cm^{-2} current density was observed by in-situ optical microscopy.

Table S1. The RTC and RTC ratio of Zn anode with different crystal surfaces in different electrolytes.

	Zn(002)	**Zn(100)**	**Zn(101)**	**$RTC_{(002)}$/ $RTC_{(100)}$**	**$RTC_{(002)}$/ $RTC_{(101)}$**
D2	2.04	7.78	19.98	0.26	0.10
D4	0.68	6.85	18.53	0.10	0.04
D7	2.44	5.39	12.23	0.45	0.20
D10	1.94	9.59	16.01	0.20	0.12
D15	2.55	12.21	13.98	0.21	0.18

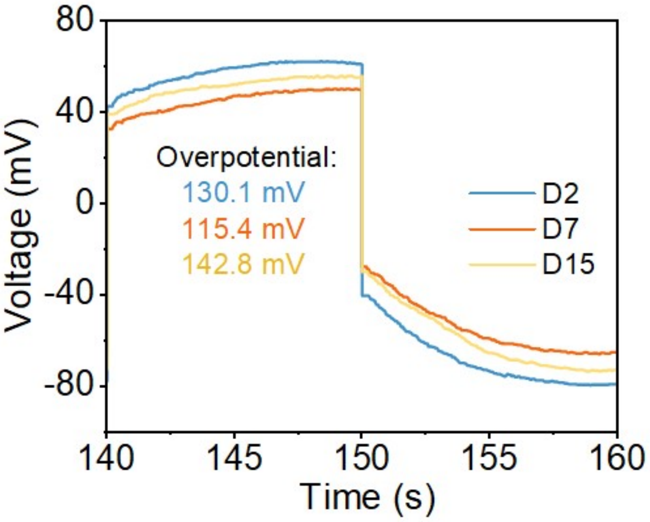

Fig. S11. Details of polarization characteristics of Zn//Cu asymmetric cell in D2, D7 and D15.

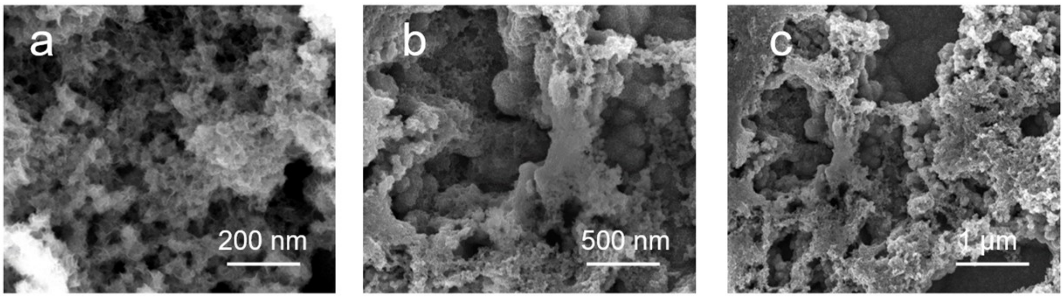

Fig. S12. SEM of MnO_2 cathode at (a) 200nm, (b) 500nm and (c) 1µm.

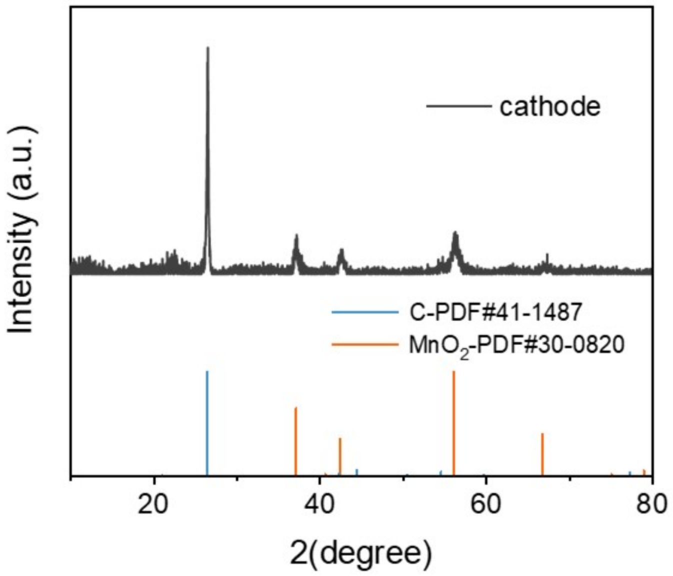

Fig. S13. XRD of MnO_2 cathode.